arXiv:2103.15378v2 [cond-mat.mes-hall] 17 Aug 2021

Bilayer graphene encapsulated within monolayers of WS_2 or $Cr_2Ge_2Te_6$: Tunable proximity spin-orbit or exchange coupling

Klaus Zollner[1,*] and Jaroslav Fabian[1]

[1] *Institute for Theoretical Physics, University of Regensburg, 93053 Regensburg, Germany*

(Dated: August 18, 2021)

Van der Waals (vdW) heterostructures consisting of bilayer graphene (BLG) encapsulated within monolayers of strong spin-orbit semiconductor WS_2 or ferromagnetic semiconductor $Cr_2Ge_2Te_6$ (CGT), are investigated. By performing realistic first-principles calculations we capture the essential BLG band structure features, including layer- and sublattice-resolved proximity spin-orbit or exchange couplings. For different relative twist angles (0 or 60°) of the WS_2 layers, and the magnetizations (parallel or antiparallel) of the CGT layers, with respect to BLG, the low energy bands are found and characterized by a series of fit parameters of model Hamiltonians. These effective models are then employed to investigate the tunability of the relevant energy dispersions by a gate field. For WS_2/BLG/WS_2 encapsulation we find that twisting allows to turn off the spin splittings away from the K points, due to opposite proximity-induced valley-Zeeman couplings in the two sheets of BLG. Close to the K points the electron spins are polarized out of the plane. This polarization can be flipped by applying a gate field. As for magnetic CGT/BLG/CGT structures, we realize the recently proposed spin-valve effect, whereby a gap opens for antiparallel magnetizations of the CGT layers. Furthermore, we find that for the antiferromagnetic orientation the electron states away from K have vanishingly weak proximity exchange, while the states close to K remain spin polarized in the presence of an electric field. The induced magnetization can be flipped by changing the gate field. These findings should be useful for spin transport, spin filtering, and spin relaxation anisotropy studies of BLG-based vdW heterostructures.

Keywords: spintronics, bilayer graphene, heterostructures, proximity spin-orbit coupling, proximity exchange

INTRODUCTION

Layered two-dimensional (2D) van der Waals (vdW) materials have become indispensable for exploring new functionalities in electronics and spintronics [1–3]. The fact that distinct 2D materials mutually influence each other in vdW heterostructures via proximity effects [4] has opened venues for novel device designs at the nanoscale [5–7]. It has been shown that several interactions, such as superconductivity [8, 9], magnetism [10–13], and spin-orbit coupling (SOC) [14–17], can be induced on demand, while simultaneously each individual layer maintains its characteristic properties. Moreover, these proximity-induced spin interactions can be further modulated by gating and twisting [12, 18–27].

In this context, bilayer graphene (BLG) has emerged as a model playground for gate- and twist-tunable correlated physics [28–46] as well as for layer-dependent proximity-induced spin interactions [11, 47–55]. Two sheets of graphene stacked at a small twist angle can become insulating, ferromagnetic [33, 38, 41], or superconducting [28–32] under certain filling factors of the Moiré Brillouin zone. By tuning the twist angle, one controls the interlayer coupling, thereby tailoring electronic and optical properties of BLG [56]. In addition, also other microscopic details are highly important, such as strain, dielectric environment, and the alignment to encapsulation layers [31, 33, 35, 36, 45].

Also proximity effects can induce spin interactions in BLG [4, 10, 11, 14–16, 18, 20, 25, 47–49, 57–73]. As theoretically predicted by first-principles calculations [47] and recently confirmed via penetration field capacitance measurements [52] and mesoscopic transport [54], a transition-metal dichalcogenide (TMDC) in proximity to BLG strongly enhances the SOC of the adjacent graphene layer only. By applying a gate voltage, one can then fully electrically turn on and off the SOC of the BLG conduction electrons. Proximity effects even allow for swapping spin interactions (SOC and exchange) in vdW structures, such as BLG encapsulated between a ferromagnetic and a strong spin-orbit layer [49]. Such a "bottom-up" approach to vdW engineering, building more complex structures beyond bilayers, is just starting to reveal its enormous potential for tailoring charge, spin, and optical properties of 2D materials.

Particularly interesting are the recent experimental findings by Lin et al. [50], who studied the combined effects of strong electronic correlations and SOC in WSe_2 proximitized magic-angle twisted BLG. Remarkably, the proximity Rashba and valley Zeeman SOC induces orbital magnetism without the need for a rotational alignment to a hexagonal boron-nitride substrate [33, 36]. In addition, WSe_2 can help to stabilize superconductivity in twisted BLG [30], emphasizing the role of the dielectric environment. Also for the interpretation of such experimental findings it is useful to have a quantitative knowledge about proximity effects in BLG. For example, as demonstrated in Ref. [52], the measured penetration field capacitance of WSe_2 encapsulated BLG could be nicely related to model calculations, including proximity-

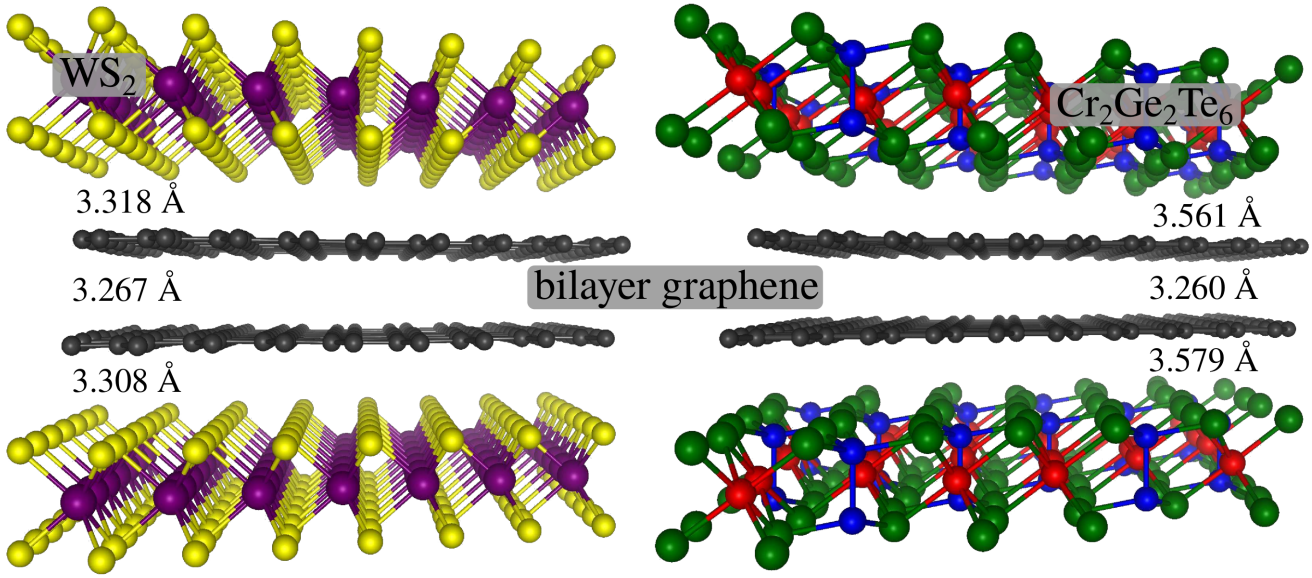


FIG. 1. Geometries of the encapsulated BLG heterostructures. Left: WS_2 encapsulated BLG, Right: CGT encapsulated BLG. The relaxed interlayer distances are also indicated.

induced valley-Zeeman SOC of opposite sign on the two graphene layers.

In this work, we consider BLG encapsulated either by monolayers of the strong spin-orbit semiconductor WS_2 or by monolayers of the ferromagnetic semiconductor $Cr_2Ge_2Te_6$ (CGT). In such vdW heterostructures, BLG preserves a great degree of autonomy of its electronic structure, but both graphene layers experience proximity effects (SOC by WS_2 or exchange coupling by CGT). In general, also other transition-metal dichalcogenides (MoS_2, $MoSe_2$, and WSe_2) or 2D magnets (CrI_3, $MnPSe_3$) are possible choices. Here, WS_2 and CGT serve as exemplary materials, inducing the spin interactions in the graphene layers. In the case of WS_2 encapsulation, and when all layers are perfectly aligned (0° twist angle), we find that the induced SOC is of valley-Zeeman type ($\lambda_{\rm I}^{\rm A} \approx -\lambda_{\rm I}^{\rm B} \approx 1$ meV) and the same for both graphene layers. By twisting the top WS_2 layer by 60°, with respect to the underlying BLG/WS_2 structure, the valley-Zeeman SOC of the top graphene layer switches sign ($\lambda_{\rm I}^{\rm A} \to -\lambda_{\rm I}^{\rm A}$, $\lambda_{\rm I}^{\rm B} \to -\lambda_{\rm I}^{\rm B}$). Rotating the top WS_2 layer by 60°, we effectively switch the A and B sublattice of the underlying graphene layer. This has dramatic consequences for the low energy bands of the WS_2 encapsulated BLG, under zero external transverse electric field. The bands are spin-split, gapless, and s_z spin-polarized for 0° twist angle, while for 60°, they remain nearly unsplit and exhibit a band gap. The reason is the sublattice- and layer-polarized low energy band structure of BLG in combination with the short-range and layer-resolved proximity-induced valley-Zeeman SOC, that can be controlled by the twist angle. Our first-principles results explicitly prove the capacitance measurements on TMDC encapsulated BLG performed by Island et al. [52].

Similarly, when BLG is encapsulated within two CGT monolayers, their individual magnetizations control the sign of the proximity-induced exchange coupling in the corresponding graphene layer. When both CGT layers have parallel magnetization, both graphene layers experience similar and uniform proximity exchange ($\lambda_{\rm ex}^{\rm A} \approx \lambda_{\rm ex}^{\rm B} \approx -3.5$ meV). By switching the magnetization direction of the top CGT layer, the proximity-induced exchange coupling of the adjacent graphene layer switches sign ($\lambda_{\rm ex}^{\rm A} \to -\lambda_{\rm ex}^{\rm A}$, $\lambda_{\rm ex}^{\rm B} \to -\lambda_{\rm ex}^{\rm B}$). Similar to before, the consequence for the BLG is that we can turn on and off its conductance by tuning the layer-resolved proximity exchange coupling at zero external transverse electric field. This realizes the recently proposed spin-valve vdW heterostructure [53]. A finite electric field can be used to tune the band gap, as well as spin and charge transport properties.

COMPUTATIONAL DETAILS AND GEOMETRY

In the following we consider BLG in Bernal stacking, which is encapsulated within two layers of WS_2 or CGT, see Fig. 1. Initial atomic structures are set up with the atomic simulation environment (ASE) [74] and visualized with VESTA software [75]. For the first-principles calculations we use 5×5 supercells of BLG, $\sqrt{3} \times \sqrt{3}$ CGT supercells, and 4×4 supercells of WS_2. In the case of WS_2 encapsulation, we stretch the lattice constant of BLG by roughly 2% from 2.46 Å to 2.5 Å and the WS_2 lattice constant is compressed by about 1% from 3.153 Å [76] to 3.125 Å. In the case of CGT encapsulation, we keep

the lattice constant of graphene unchanged at $a = 2.46$ Å and stretch the CGT lattice constant by roughly 4% from 6.8275 Å [77] to 7.1014 Å.

The electronic structure calculations and structural relaxations of the BLG-based heterostructures are performed by density functional theory (DFT) [78] with QUANTUM ESPRESSO [79]. Self-consistent calculations are performed with the k-point sampling of $12 \times 12 \times 1$ ($9 \times 9 \times 1$) in the case of CGT (WS_2) encapsulation to get converged results for the proximity-induced exchange (SOC). We use an energy cutoff for the charge density of 500 Ry, and the kinetic energy cutoff for wavefunctions is 60 Ry for the scalar relativistic pseudopotentials with the projector augmented wave method [80] with the Perdew-Burke-Ernzerhof exchange correlation functional [81]. In the case of CGT encapsulation, we perform open shell calculations that provide the spin polarized ground state and proximity exchange coupling. In addition, a Hubbard parameter of $U = 1$ eV is used for Cr d-orbitals, similar to recent calculations [11, 82]. In the case of WS_2 encapsulation, we use the relativistic versions of the pseudopotentials, to capture (proximity) SOC effects.

For the relaxation of the heterostructures, we add vdW corrections [83, 84] and use quasi-newton algorithm based on trust radius procedure. Dipole corrections [85] are also included to get correct band offsets and internal electric fields. In order to simulate quasi-2D systems, we add a vacuum of 20 Å, to avoid interactions between periodic images in our slab geometries. Only the WS_2/BLG/WS_2 structure with 0° twist angles, as well as the CGT/BLG/CGT structure with parallel magnetizations, are relaxed. To determine the interlayer distances, the atoms of BLG and WS_2 are allowed to relax only in their z positions (vertical to the layers), and the atoms of CGT are allowed to move in all directions, until all components of all forces are reduced below 10^{-3} [Ry/a_0], where a_0 is the Bohr radius. When we then twist the top WS_2 layer by 60°, or flip the magnetization of the top CGT layer, no further structural relaxation is performed.

The obtained interlayer distances are summarized in Fig. 1 and are similar to previous reports [11, 47]. Since we have assumed perfectly aligned individual layers, the full heterostructures still have C_3 symmetry after relaxation. In addition, the relaxed structures are nearly, but not fully symmetric regarding interlayer distances. The reason is that the precise atomic registries (stackings) of top and bottom encapsulation layer, with respect to their corresponding graphene sheet, are not exactly the same.

MODEL HAMILTONIAN

Here we present the Hamiltonian used to model the low energy bands of the encapsulated BLG structures. The basis states are $|C_{A1},\uparrow\rangle$, $|C_{A1},\downarrow\rangle$, $|C_{B1},\uparrow\rangle$, $|C_{B1},\downarrow\rangle$, $|C_{A2},\uparrow\rangle$, $|C_{A2},\downarrow\rangle$, $|C_{B2},\uparrow\rangle$, and $|C_{B2},\downarrow\rangle$. In this basis the Hamiltonian is (see also Refs. 49 and 86)

$$\mathcal{H} = \mathcal{H}_{\rm orb} + \mathcal{H}_{\rm soc} + \mathcal{H}_{\rm ex} + \mathcal{H}_{\rm R} + E_D, \tag{1}$$

$$\mathcal{H}_{\rm orb} = \begin{pmatrix} \Delta + V & \gamma_0 f(\boldsymbol{k}) & \gamma_4 f^*(\boldsymbol{k}) & \gamma_1 \\ \gamma_0 f^*(\boldsymbol{k}) & V & \gamma_3 f(\boldsymbol{k}) & \gamma_4 f^*(\boldsymbol{k}) \\ \gamma_4 f(\boldsymbol{k}) & \gamma_3 f^*(\boldsymbol{k}) & -V & \gamma_0 f(\boldsymbol{k}) \\ \gamma_1 & \gamma_4 f(\boldsymbol{k}) & \gamma_0 f^*(\boldsymbol{k}) & \Delta - V \end{pmatrix} \otimes s_0, \tag{2}$$

$$\mathcal{H}_{\rm soc} + \mathcal{H}_{\rm ex} + \mathcal{H}_{\rm R} = \begin{pmatrix} (\tau\lambda_{\rm I}^{\rm A1} - \lambda_{\rm ex}^{\rm A1})s_z & 2{\rm i}\lambda_{\rm R1}s_-^\tau & 0 & 0 \\ -2{\rm i}\lambda_{\rm R1}s_+^\tau & (-\tau\lambda_{\rm I}^{\rm B1} - \lambda_{\rm ex}^{\rm B1})s_z & 0 & 0 \\ 0 & 0 & (\tau\lambda_{\rm I}^{\rm A2} - \lambda_{\rm ex}^{\rm A2})s_z & 2{\rm i}\lambda_{\rm R2}s_-^\tau \\ 0 & 0 & -2{\rm i}\lambda_{\rm R2}s_+^\tau & (-\tau\lambda_{\rm I}^{\rm B2} - \lambda_{\rm ex}^{\rm B2})s_z \end{pmatrix}. \tag{3}$$

Here, γ_j, $j = \{0, 1, 3, 4\}$, describe intra- and interlayer hoppings in BLG, as schematically illustrated in Fig. 2. The parameter γ_0 is the nearest neighbor intralayer hopping, similar to monolayer graphene, while γ_1 is the direct interlayer hopping. The parameters γ_3 and γ_4 describe indirect hoppings between the layers. The vertical hopping γ_1 connects only 2 atoms and therefore it appears without structural function in the Hamiltonian. In contrast, the other hoppings couple an atom to three corresponding nearest neighbor partner atoms, hence they appear with structural function, where we use the linearized version, $f(\boldsymbol{k}) = -\frac{\sqrt{3}a}{2}(\tau k_x - {\rm i}k_y)$, valid in the vicinity of the K points [87]. The graphene lattice constant is a and the Cartesian wave vector components k_x and k_y are measured with respect to $\pm K$ for the valley indices $\tau = \pm 1$. In addition, the lower (upper) graphene layer is placed in the potential V ($-V$). The parameter Δ describes the asymmetry in the energy shift of the bonding and antibonding states, which arises due to the interlayer coupling γ_1. The Pauli spin matrices are s_i, with $i = \{0, x, y, z\}$, and $s_\pm^\tau = \frac{1}{2}(s_x \pm {\rm i}\tau s_y)$.

The parameters $\lambda_{\rm I}$ ($\lambda_{\rm ex}$) describe the proximity-

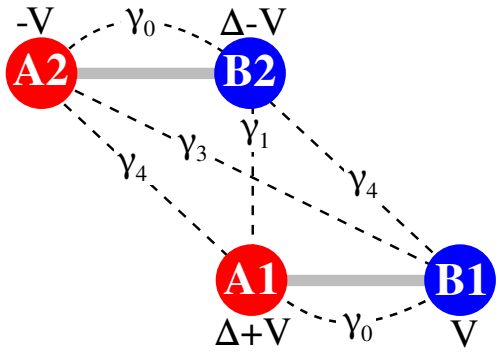


FIG. 2. Schematic illustration of the BLG lattice, showing the relevant intra- and interlayer hoppings γ_j, $j = \{0, 1, 3, 4\}$ (dashed lines). In addition, the lower (upper) graphene layer is placed in the potential V $(-V)$, while the asymmetry Δ arises due to γ_1.

induced intrinsic SOC (exchange) of the corresponding layer and sublattice atom ($C_{A1}, C_{B1}, C_{A2}, C_{B2}$). The intrinsic SOC parameters are also present in pristine BLG and on the order of 10 μeV [86]. However, they will be strongly renormalized, because of the surrounding WS_2 layers providing an extra (on the meV scale) amount of SOC for the effective p_z-orbitals. The exchange couplings are due to surrounding magnetic materials, giving rise to similar band splittings as the SOC parameters, but breaking time-reversal symmetry. The parameters λ_{R1} and λ_{R2} are the Rashba couplings of the two individual graphene layers. In pristine BLG, the two Rashba parameters have the same value but are opposite in sign, because the graphene layers feel each others presence. When an electric field is applied across BLG, the Rashba couplings can become dissimilar. However, the surrounding WS_2 layers can strongly enhance the Rashba couplings, just as for monolayer graphene [15].

To capture doping effects from the calculations, we introduce another parameter E_D, which leads to an energy shift on the model band structure and we call it the Dirac point energy. To extract the fit parameters form the DFT, we employ a least-squares routine, taking into account band energies, splittings, and spin expectation values. First, we extract the orbital parameters, γ_j, Δ, and V. Once they are fixed, we extract the spin-orbit or exchange parameters, depending on the encapsulation layers.

BAND STRUCTURE, FIT RESULTS, AND GATE TUNABILITY

WS_2 encapsulated BLG

The first case that we address is the WS_2 encapsulated BLG. Here, SOC is included in the calculation, since we are interested in proximity-induced SOC effects, that are present in both graphene layers. The calculated band structure is shown in Fig. 3(a). The dispersion features four s_z-polarized parabolic bands near the Fermi level, that originate from BLG and which are located within the band gaps of top and bottom TMDCs. Because the layers interact via weak vdW forces, the dispersion of BLG stays perfectly intact.

Zooming in to the relevant low energy bands, see Fig. 3(b), we find perfect agreement of the first-principles calculation results with the model Hamiltonian. The fit parameters are summarized in Table I, reproducing also the BLG high energy bands, splittings, and spin expectation values (see Supplemental Material [88]). We know from previous calculations [11, 47, 49], that a substrate below BLG induces a dipole field in BLG, similarly to an external electric field. In both cases, a band gap will open in the low energy dispersion. Here, the WS_2 encapsulated structure is roughly z-mirror symmetric, and nearly no dipole field is present. Hence, the orbital band gap is closed. In addition, both graphene layers experience the same amount of proximity-induced valley-Zeeman type SOC, see Table I. In addition, they experience almost opposite Rashba SOC, since the bottom (top) graphene layer has the WS_2 as substrate (capping) layer. The small difference in value arises due to slightly different interlayer distances. To understand this, one has to see each graphene layer individually, being encapsulated by a WS_2 layer and another graphene layer. For bare BLG, we know that the intrinsic Rashba SOC is small (5 μeV) [86]. It is then the WS_2 layer, being responsible for strongly deforming the p_z-orbitals along z-direction, giving rise to significant Rashba SOC [15]. This should not to be mixed up with the Rashba SOC originating from electric fields [86, 89, 90]. In the Supplemental Material [88], we show the calculated charge density in real space, corresponding to the low energy bands in Fig. 3(b). We find that the non-dimer atoms are almost exclusively responsible for the bands near the Fermi level. In addition, there are small contributions from the surrounding TMDC layers, being responsible for the sizable proximity-induced SOC.

What happens if we now rotate the upper WS_2 layer by 60°? We will still have a fully C_3 symmetric heterostructure, but the layer alignment changes (remember also that we do not again relax the heterostructure after twisting). The most drastic consequence is in reciprocal space. We know that the valley-Zeeman SOC is connected to the spin-valley locking in the TMDC. When all layers are aligned (0° twist angles), the K and K' points of the individual Brillouin zones are also aligned and both graphene layers are equally proximitized. However, when the top WS_2 layer is rotated by 60°, the K point of the BLG/WS_2 substrate couples now to the K' point of the top WS_2 layer, and vice versa. Regarding experiment, there are now techniques to stack the layers under well controlled twist angles [56, 91]. We want to know, what is the consequence for the low energy BLG bands?

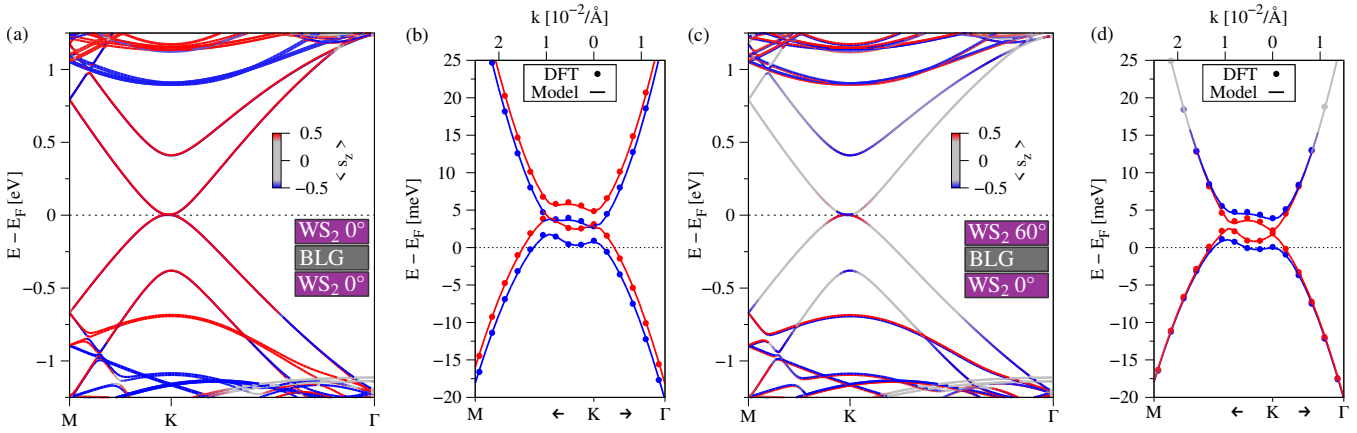


FIG. 3. (a) Band structure of WS_2 encapsulated BLG along the $M-K-\Gamma$ path. The color of the bands corresponds to the s_z spin expectation value. In the inset, we schematically illustrate the heterostructure, where both WS_2 layers have 0° twist angle with respect to BLG. (b) Zoom to the calculated low energy bands (symbols) around the K point, corresponding to the band structure in (a), with a fit to the model Hamiltonian (solid lines). [(c) and (d)] Same as [(a) and (b)] but when the top WS_2 layer is rotated by 60° twist angle with respect to the remaining BLG/WS_2 structure, as schematically illustrated in (c).

In Fig. 3(c) we show the global band structure for the 60° scenario. Overall, the dispersion is nearly the same as before, but the BLG bands are only s_z-polarized near the K point. Away from the K point, bands show an in-plane spin polarization (they appear gray in our color scale). In addition, if we zoom in to the fine structure, see Fig. 3(d), we find that the low energy bands are nearly unsplit away from the K point. The reason is that the low energy bands are formed by non-dimer atoms C_{B1} and C_{A2} from the individual graphene layers [86, 92], now experiencing Rashba and opposite valley-Zeeman SOC, see the fit parameters in Table I. At the K point, the bands have a clear sublattice and layer character because of the small intrinsic dipole field. The band splittings and polarizations are dominated by the intrinsic SOC parameters. Therefore, bands are split and s_z-polarized.

However, away from the K point the bands are formed equally by non-dimer atoms, having opposite valley-Zeeman couplings, effectively cancelling each other. Hence, bands are nearly unsplit and start to get in-plane polarized due to the sizable Rashba SOC, dominating the band polarizations. Again, we find perfect agreement of the first-principles calculation results with the model Hamiltonian, see Fig. 3(d), employing the fit parameters in Table I. The vanishing of the valley-Zeeman coupling for states away from the K point is expected to decrease the spin relaxation anisotropy (spin lifetime ratio of out-of-plane to in-plane spins) to 50%, characteristic for (residual) Rashba interactions only, deviating from the giant anisotropies predicted for large valley-Zeeman splittings [93]. The gate field should then restore the giant anisotropies (10-100), by introducing valley-Zeeman couplings via layer polarization.

TABLE I. The fit parameters of the model Hamiltonian $\mathcal{H}$ for the WS_2 and the CGT encapsulated BLG structures. For the WS_2 encapsulation, we consider the top WS_2 layer to be twisted by either 0° or 60°. In the case of CGT encapsulation, we consider parallel (P) or antiparallel (AP) magnetizations of the two CGT layers.

system	WS_2 (0°)	WS_2 (60°)	CGT (P)	CGT (AP)
γ_0 [eV]	2.444	2.444	2.519	2.524
γ_1 [eV]	0.395	0.395	0.387	0.387
γ_3 [eV]	−0.288	−0.282	−0.296	−0.295
γ_4 [eV]	−0.170	−0.170	−0.189	−0.189
V [meV]	−0.951	−1.103	−0.495	−0.423
Δ [meV]	12.331	13.346	9.303	9.255
λ_{R1} [meV]	0.300	0.295	0	0
λ_{R2} [meV]	−0.277	−0.222	0	0
λ_I^{A1} [meV]	1.039	1.006	0	0
λ_I^{B1} [meV]	−1.090	−0.901	0	0
λ_I^{A2} [meV]	1.029	−0.802	0	0
λ_I^{B2} [meV]	−1.007	1.072	0	0
λ_{ex}^{A1} [meV]	0	0	−3.447	−3.254
λ_{ex}^{B1} [meV]	0	0	−3.625	−3.460
λ_{ex}^{A2} [meV]	0	0	−3.447	3.254
λ_{ex}^{B2} [meV]	0	0	−3.625	3.460
E_D [meV]	2.815	1.928	0.987	1.051
dipole [debye]	0.020	0.037	0.051	0.054

CGT encapsulated BLG

Now, we consider CGT encapsulated BLG. Here, SOC is switched off in the calculation, because we are interested in bare proximity exchange parameters. In addi-

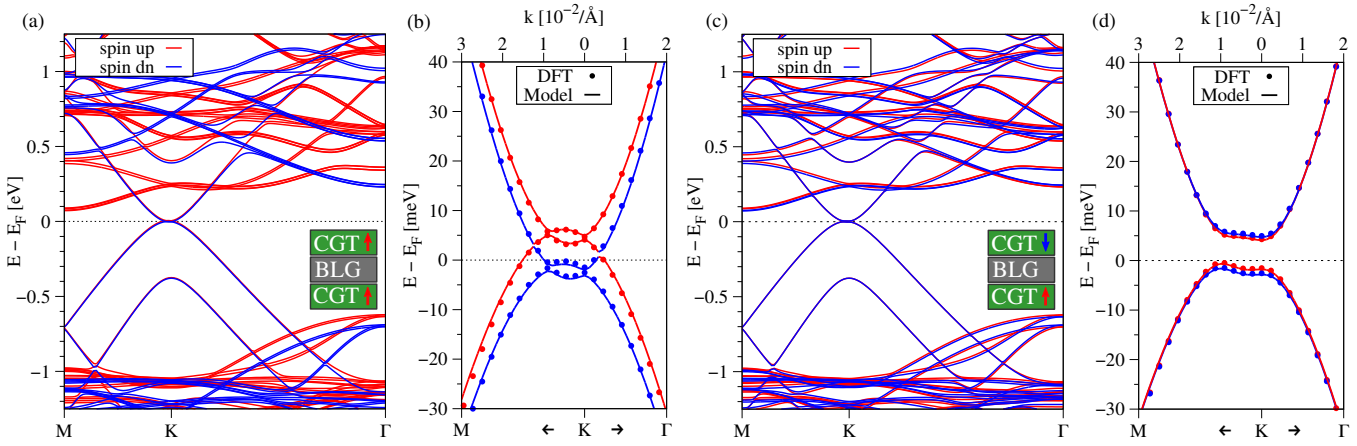


FIG. 4. (a) Band structure of CGT encapsulated BLG along the $M-K-\Gamma$ path. Bands in red (blue) correspond to spin up (spin down). In the inset, we schematically illustrate the heterostructure, where both CGT layers have parallel magnetization (red arrows), pointing along the z direction. (b) Zoom to the calculated low energy bands (symbols) around the K point, corresponding to the band structure in (a), with a fit to the model Hamiltonian (solid lines). (c,d) Same as (a,b) but for antiparallel magnetization of the two CGT layers [bottom layer along z, top layer along $-z$, as schematically illustrated in (c)].

tion, we know that proximity SOC in graphene from CGT is small compared to its proximity exchange [59]. Also in this case, both graphene layers are getting proximitized, and the valence and conduction band of BLG are spin split. Depending on the magnetization directions of the two individual CGT layers, different low energy band structures can be realized. Our results show that in the ferromagnetic configuration, where the magnetizations of both CGT layers point along the z direction, both graphene layers are getting equally proximitized, see Fig. 4(a,b). This is especially reflected in the model exchange parameters, $\lambda_{\rm ex}$, in Table I, which are equal in sign and magnitude for all C sublattice atoms. Again, the CGT/BLG/CGT sandwich structure is more or less z-mirror symmetric and the built-in dipole field is almost zero. Consequently, the orbital band gap of BLG is closed, see Fig. 4(b), which is reflected in the small potential parameter V.

For the antiferromagnetic configuration, in which the magnetization of the bottom (top) CGT layer points along the z ($-z$) direction, proximity exchange effects are still present, but the sign of the exchange coupling for the top graphene layer changes. Consequently, the spin splitting will be of similar magnitude, but of opposite sign, as also reflected in the fitted parameters in Table I. Since we have switched the magnetization of one CGT layer, the global band structure is still similar to the ferromagnetic case, compare Fig. 4(a) and Fig. 4(c), but the bands corresponding to the upper CGT layer have switched their spin polarization. Most remarkably, the fine structure near the K point reveals a sizable band gap of about 5 meV, such that no bands cross the Fermi level, see Fig. 4(d). In this case, it is not an intrinsic dipole field that is responsible for the gap opening, but rather the unique sublattice- and layer-polarized low energy band structure of BLG itself, being subject to layered antiferromagnetic proximity exchange.

Our CGT/BLG/CGT geometry is similar to the recently proposed CrI_3/BLG/CrI_3 spin-valve heterostructure [53], in which the in-plane conductance can be controlled by switching the magnetic configuration. Indeed, the spin-split low energy bands cross the Fermi level and the system is conductive in the ferromagnetic case, see Fig. 4(b), while in the antiferromagnetic case, see Fig. 4(d), no bands cross the Fermi level and the system is insulating. The advantage of our presented structure is that only the bands of the proximitized BLG are present at the Fermi level, while for the CrI_3/BLG/CrI_3 structure also bands originating from the CrI_3 layers reside near the Fermi level [53].

We want to point out that this switching mechanism works for our symmetrical heterostructures, because $V \approx 0$ at zero external electric field. In experiment, when BLG is asymmetrically encapsulated, e. g., with some additional substrate material, one needs to tune the total electric field (built-in plus external) such that $V \approx 0$.

Gate tunable low energy bands

We now turn to the gate tunability of the low energy bands. As we know, an external electric field can be used to tune the band gap of BLG [11, 47, 49, 86]. We exploit the model Hamiltonian, along with the zero external field parameters, listed in Table I, to calculate the electric field behavior. We do not perform any additional first-principles calculations here. From previous results [49],

we know that the electric field behavior can be modelled realistically by tuning the parameter V only. For the model calculations, we also set the Dirac point energy $E_D = 0$, since doping effects seem not to play a role, as the above first-principles results show.

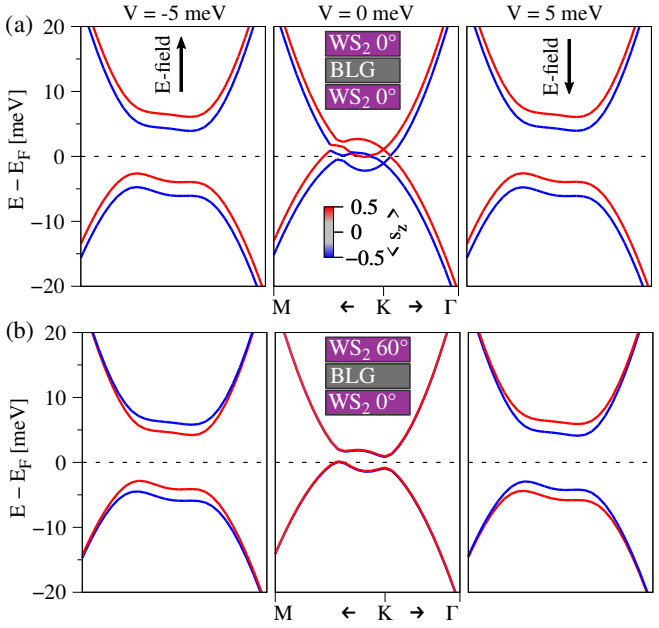


FIG. 5. Calculated low energy model band structures employing the fit parameters from Table I for the case of WS_2 encapsulation, when the top WS_2 layer is rotated by (a) 0° and (b) 60°. The insets schematically illustrate the situations, as in Fig. 3. From left to right, we tune the parameter V from −5 meV to 5 meV, to simulate an external electric field, as indicated by the arrows.

We restrict ourselves to three relevant cases, $V = -5$, 0, and 5 meV, corresponding to external electric fields of about 0.75, 0, and −0.75 V/nm. A particularly interesting case is, when $V = 0$, i. e., both graphene layers are at the same potential, equally contributing to the low energy bands at the K point. In our heterostructure calculations, a small asymmetry in the interlayer distances remains from the relaxation, leading to a finite intrinsic dipole and $V \neq 0$, see Table I.

WS_2 encapsulated BLG

In Fig. 5, we summarize the model calculation results, when employing an external electric field, for WS_2 encapsulated BLG. For the 0° twist angle and zero electric field ($V = 0$), we find that the low energy bands are equally split, s_z polarized and cross the Fermi level, similar to Fig. 3(b). When an electric field is applied ($V \neq 0$), a band gap opens. Independent of the field direction, the low energy bands are the same, since both graphene layers experience the same valley-Zeeman SOC. For the 60° twist angle and zero electric field, the bands already exhibit a gap and remain nearly unsplit. The origin is that the individual valley-Zeeman SOCs from the two graphene layers are now almost opposite, nearly canceling each other. The presented results are in perfect agreement with recent capacitance measurements and model considerations of WSe_2 encapsulated BLG [52].

In general, whenever the proximity SOCs of top and bottom graphene layers cancel each other, the bands remain spin degenerate for zero electric field. A finite electric field opens the band gap, just as before. But now, depending on the field direction, *the polarization of the two innermost bands can be switched, potentially important for spin-filtering purposes.* However, one could argue that the band splittings are small (few meV), which is a drawback for practical usage of spin filtering. Nevertheless, one is not limited to our scenario of WS_2 encapsulation and can use other 2D materials that induce a more sizable SOC in the graphene layers. The working principle remains the same.

CGT encapsulated BLG

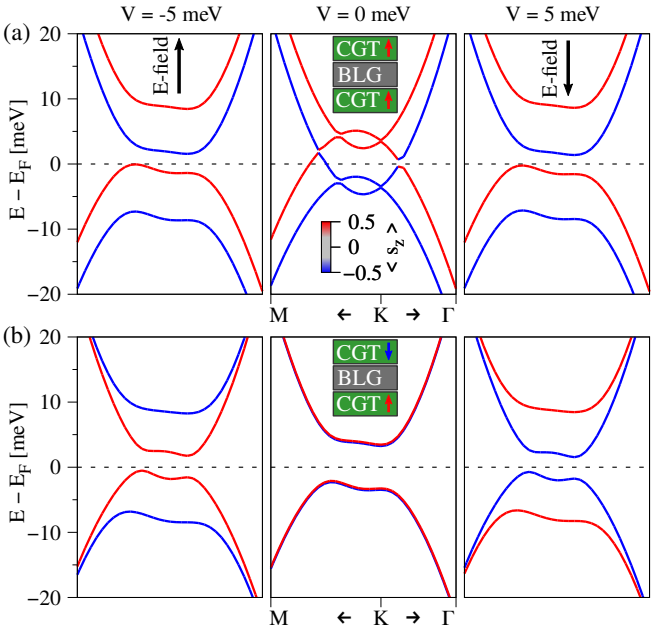


FIG. 6. Calculated low energy model band structures employing the fit parameters from Table I for the case of CGT encapsulation, for (a) parallel (P) and (b) antiparallel (AP) magnetizations of the two CGT layers. The insets schematically illustrate the situations, as in Fig. 4. From left to right, we tune the parameter V from −5 meV to 5 meV, to simulate an external electric field, as indicated by the arrows.

In Fig. 6, we summarize the model calculation results, when employing an external electric field, for CGT encapsulated BLG. In the ferromagnetic case, the low energy

bands can be tuned symmetrically with the field, independent of the field direction, see Fig. 6(a). The reason is, that both graphene layers experience equal proximity effects. This is also, why at zero field, the bands remain split. In strong contrast, in the antiferromagnetic case, and at zero field, the bands are also formed equally by both graphene layers, but with opposite sign of proximity exchange. The couplings effectively cancel each other and bands remain nearly unsplit. Because of this layered antiferromagnetic proximity exchange, *switching between positive and negative electric field allows to flip the spin-polarization of the two low energy bands*, closest to the Fermi level. Consequently, the relative magnetization of the two CGT layers can be used to turn on and off the in-plane conductance at zero external field. In the antiferromagnetic case, an external electric field can be used to control spin filtering. Already here, we can see that the band splittings are much larger than in the WS_2 encapsulation case, making the CGT-encapsulated structure more favorable for practical usage of spin filtering. With regard to switching on and off the in-plane conductance, one could argue that the gap (≈ 5 meV) is rather small for practical purposes. However, since the size of the gap is proportional to the exchange couplings, one can simply use another ferromagnetic semiconductor that induces a more sizable proximity exchange in the graphene layers.

In addition, we think that few meV of electronic gaps can be easily resolved now in experiments. For example recent capacitance [52] and magneto-transport [51, 54] measurements were able to resolve such gaps in proximitized BLG and could relate this to similar band structure results that we show.

SUMMARY

In summary, we have calculated the electronic structure of WS_2 or CGT encapsulated BLG from first principles. By employing a model Hamiltonian, we were able to reproduce the relevant low energy bands of BLG using suitable fit parameters. The gate tunability of the bands was studied on a model level. Depending on the encapsulation material, either valley-Zeeman SOC or exchange coupling is induced in both graphene layers. Depending on the twist angle (magnetization direction) of one WS_2 (CGT) layer with respect to the remaining heterostructure, the corresponding proximity-induced valley-Zeeman SOC (exchange coupling) in the adjacent graphene layer can be switched in sign. These tunable layer-resolved proximity effects in combination with the unique sublattice character of the BLG low energy bands, allows to turn on and off the in-plane conductance at zero external electric field. A finite electric field can be used to further tailor the spin and charge transport properties.

Our results show that not only proximity effects influence the low energy characteristics of BLG, but also the alignment and relative magnetization of the surrounding layers is important. In general, the presented findings should be also valid when replacing the AB-stacked BLG with magic-angle twisted BLG. The splitting of the flat bands may then also be turned on and off, potentially leading to very different phase diagrams when tuning the filling factor of the Moiré Brillouin zone. This has been already demonstrated for a single WSe_2 substrate in proximity to twisted BLG [30, 50]. The next step would be the encapsulation within strong spin-orbit and/or ferromagnetic semiconductors.

This work was funded by the Deutsche Forschungsgemeinschaft (DFG, German Research Foundation) SFB 1277 (Project No. 314695032), SPP 2244 (Project No. 443416183), and the European Union Horizon 2020 Research and Innovation Program under contract number 881603 (Graphene Flagship).

* klaus.zollner@physik.uni-regensburg.de

[1] Wei Han, Roland K Kawakami, Martin Gmitra, and Jaroslav Fabian, "Graphene spintronics," Nat. Nanotechnol. **9**, 794 (2014).

[2] Jaroslav Fabian, Alex Matos-Abiague, Christian Ertler, Peter Stano, and Igor Zutic, "Semiconductor spintronics," Acta Phys. Slov. **57**, 565 (2007).

[3] A. Avsar, H. Ochoa, F. Guinea, B. Özyilmaz, B. J. van Wees, and I. J. Vera-Marun, "Colloquium: Spintronics in graphene and other two-dimensional materials," Rev. Mod. Phys. **92**, 021003 (2020).

[4] Igor Zutic, Alex Matos-Abiague, Benedikt Scharf, Hanan Dery, and Kirill Belashchenko, "Proximitized materials," Mater. Today **22**, 85 (2019).

[5] Cheng Gong and Xiang Zhang, "Two-dimensional magnetic crystals and emergent heterostructure devices," Science **363**, eaav4450 (2019).

[6] Hui Li, Shuangchen Ruan, and Yu-Jia Zeng, "Intrinsic Van Der Waals Magnetic Materials from Bulk to the 2D Limit: New Frontiers of Spintronics," Adv. Mater. **31**, 1900065 (2019).

[7] David L. Cortie, Grace L. Causer, Kirrily C. Rule, Helmut Fritzsche, Wolfgang Kreuzpaintner, and Frank Klose, "Two-Dimensional Magnets: Forgotten History and Recent Progress towards Spintronic Applications," Advanced Functional Materials **30**, 1901414 (2019).

[8] Jing Li, Han-Bing Leng, Hailong Fu, Kenji Watanabe, Takashi Taniguchi, Xin Liu, Chao-Xing Liu, and Jun Zhu, "Superconducting proximity effect in a transparent van der waals superconductor-metal junction," Phys. Rev. B **101**, 195405 (2020).

[9] Rai Moriya, Naoto Yabuki, and Tomoki Machida, "Superconducting proximity effect in a $Nbse_2$/graphene van der waals junction," Phys. Rev. B **101**, 054503 (2020).

[10] Klaus Zollner, Martin Gmitra, Tobias Frank, and Jaroslav Fabian, "Theory of proximity-induced exchange coupling in graphene on hBN/(Co, Ni)," Phys. Rev. B **94**, 155441 (2016).

[11] Klaus Zollner, Martin Gmitra, and Jaroslav Fabian,

"Electrically tunable exchange splitting in bilayer graphene on monolayer $Cr_2X_2Te_6$ with X = Ge, Si, and Sn," New J. Phys. **20**, 073007 (2018).

[12] Klaus Zollner, Paulo E. Faria Junior, and Jaroslav Fabian, "Proximity exchange effects in $MoSe_2$ and WSe_2 heterostructures with CrI_3: Twist angle, layer, and gate dependence," Phys. Rev. B **100**, 085128 (2019).

[13] Klaus Zollner, Paulo E. Faria Junior, and Jaroslav Fabian, "Giant proximity exchange and valley splitting in transition metal dichalcogenide/hBN/(Co, Ni) heterostructures," Phys. Rev. B **101**, 085112 (2020).

[14] Martin Gmitra and Jaroslav Fabian, "Graphene on transition-metal dichalcogenides: A platform for proximity spin-orbit physics and optospintronics," Phys. Rev. B **92**, 155403 (2015).

[15] Martin Gmitra, Denis Kochan, Petra Högl, and Jaroslav Fabian, "Trivial and inverted Dirac bands and the emergence of quantum spin Hall states in graphene on transition-metal dichalcogenides," Phys. Rev. B **93**, 155104 (2016).

[16] Klaus Zollner and Jaroslav Fabian, "Single and bilayer graphene on the topological insulator Bi_2Se_3: Electronic and spin-orbit properties from first principles," Phys. Rev. B **100**, 165141 (2019).

[17] Klaus Zollner and Jaroslav Fabian, "Heterostructures of graphene and topological insulators bi2se3, bi2te3, and sb2te3," physica status solidi (b) **258**, 2000081 (2021).

[18] Kenan Song, David Soriano, Aron W. Cummings, Roberto Robles, Pablo Ordejón, and Stephan Roche, "Spin Proximity Effects in Graphene/Topological Insulator Heterostructures," Nano Lett. **18**, 2033 (2018).

[19] Alessandro David, Péter Rakyta, Andor Kormányos, and Guido Burkard, "Induced spin-orbit coupling in twisted graphene–transition metal dichalcogenide heterobilayers: Twistronics meets spintronics," Phys. Rev. B **100**, 085412 (2019).

[20] Ahmet Avsar, Dmitrii Unuchek, Jiawei Liu, Oriol Lopez Sanchez, Kenji Watanabe, Takashi Taniguchi, Barbaros Özyilmaz, and Andras Kis, "Optospintronics in Graphene via Proximity Coupling," ACS Nano **11**, 11678 (2017).

[21] Talieh S Ghiasi, Alexey A Kaverzin, Patrick J Blah, and Bart J van Wees, "Charge-to-Spin Conversion by the Rashba–Edelstein Effect in Two-Dimensional van der Waals Heterostructures up to Room Temperature," Nano Lett. **19**, 5959 (2019).

[22] L Antonio Benitez, Williams Savero Torres, Juan F Sierra, Matias Timmermans, Jose H Garcia, Stephan Roche, Marius V Costache, and Sergio O Valenzuela, "Tunable room-temperature spin galvanic and spin Hall effects in van der Waals heterostructures," Nat. Mater. **19**, 170 (2020).

[23] Yunqiu Kelly Luo, Jinsong Xu, Tiancong Zhu, Guanzhong Wu, Elizabeth J. McCormick, Wenbo Zhan, Mahesh R. Neupane, and Roland K. Kawakami, "Opto-valleytronic spin injection in monolayer MoS_2/few-layer graphene hybrid spin valves," Nano Lett. **17**, 3877 (2017).

[24] CK Safeer, Josep Ingla-Aynés, Franz Herling, José H Garcia, Marc Vila, Nerea Ontoso, M Reyes Calvo, Stephan Roche, Luis E Hueso, and Fèlix Casanova, "Room-temperature spin Hall effect in graphene/MoS_2 van der Waals heterostructures," Nano Lett. **19**, 1074 (2019).

[25] Franz Herling, C. K. Safeer, Josep Ingla-Aynés, Nerea Ontoso, Luis E. Hueso, and Fèlix Casanova, "Gate tunability of highly efficient spin-to-charge conversion by spin hall effect in graphene proximitized with wse2," APL Materials **8**, 071103 (2020).

[26] Abdulrhman M. Alsharari, Mahmoud M. Asmar, and Sergio E. Ulloa, "Topological phases and twisting of graphene on a dichalcogenide monolayer," Phys. Rev. B **98**, 195129 (2018).

[27] Yang Li and Mikito Koshino, "Twist-angle dependence of the proximity spin-orbit coupling in graphene on transition-metal dichalcogenides," Phys. Rev. B **99**, 075438 (2019).

[28] Yuan Cao, Valla Fatemi, Shiang Fang, Kenji Watanabe, Takashi Taniguchi, Efthimios Kaxiras, and Pablo Jarillo-Herrero, "Unconventional superconductivity in magic-angle graphene superlattices," Nature **556**, 43 (2018).

[29] Yuan Cao, Valla Fatemi, Ahmet Demir, Shiang Fang, Spencer L. Tomarken, Jason Y. Luo, Javier D. Sanchez-Yamagishi, Kenji Watanabe, Takashi Taniguchi, Efthimios Kaxiras, Ray C. Ashoori, and Pablo Jarillo-Herrero, "Correlated insulator behaviour at half-filling in magic-angle graphene superlattices," Nature **556**, 80 (2018).

[30] Harpreet Singh Arora, Robert Polski, Yiran Zhang, Alex Thomson, Youngjoon Choi, Hyunjin Kim, Zhong Lin, Ilham Zaky Wilson, Xiaodong Xu, Jiun-Haw Chu, *et al.*, "Superconductivity in metallic twisted bilayer graphene stabilized by wse 2," Nature **583**, 379–384 (2020).

[31] Petr Stepanov, Ipsita Das, Xiaobo Lu, Ali Fahimniya, Kenji Watanabe, Takashi Taniguchi, Frank HL Koppens, Johannes Lischner, Leonid Levitov, and Dmitri K Efetov, "Untying the insulating and superconducting orders in magic-angle graphene," Nature **583**, 375–378 (2020).

[32] Xiaobo Lu, Petr Stepanov, Wei Yang, Ming Xie, Mohammed Ali Aamir, Ipsita Das, Carles Urgell, Kenji Watanabe, Takashi Taniguchi, Guangyu Zhang, *et al.*, "Superconductors, orbital magnets and correlated states in magic-angle bilayer graphene," Nature **574**, 653–657 (2019).

[33] Aaron L. Sharpe, Eli J. Fox, Arthur W. Barnard, Joe Finney, Kenji Watanabe, Takashi Taniguchi, M. A. Kastner, and David Goldhaber-Gordon, "Emergent ferromagnetism near three-quarters filling in twisted bilayer graphene," Science **365**, 605–608 (2019).

[34] Rebeca Ribeiro-Palau, Changjian Zhang, Kenji Watanabe, Takashi Taniguchi, James Hone, and Cory R. Dean, "Twistable electronics with dynamically rotatable heterostructures," Science **361**, 690–693 (2018).

[35] Yu Saito, Fangyuan Yang, Jingyuan Ge, Xiaoxue Liu, Takashi Taniguchi, Kenji Watanabe, JIA Li, Erez Berg, and Andrea F Young, "Isospin pomeranchuk effect in twisted bilayer graphene," Nature **592**, 220–224 (2021).

[36] M. Serlin, C. L. Tschirhart, H. Polshyn, Y. Zhang, J. Zhu, K. Watanabe, T. Taniguchi, L. Balents, and A. F. Young, "Intrinsic quantized anomalous hall effect in a moire heterostructure," Science **367**, 900–903 (2020).

[37] C. L. Tschirhart, M. Serlin, H. Polshyn, A. Shragai, Z. Xia, J. Zhu, Y. Zhang, K. Watanabe, T. Taniguchi, M. E. Huber, and A. F. Young, "Imaging orbital ferromagnetism in a moiré chern insulator," arXiv:2006.08053 (2020).

[38] Nick Bultinck, Shubhayu Chatterjee, and Michael P. Zaletel, "Mechanism for anomalous hall ferromagnetism in

twisted bilayer graphene," Phys. Rev. Lett. **124**, 166601 (2020).
[39] Cécile Repellin, Zhihuan Dong, Ya-Hui Zhang, and T. Senthil, "Ferromagnetism in narrow bands of moiré superlattices," Phys. Rev. Lett. **124**, 187601 (2020).
[40] Ya-Hui Zhang, Dan Mao, and T. Senthil, "Twisted bilayer graphene aligned with hexagonal boron nitride: Anomalous hall effect and a lattice model," Phys. Rev. Research **1**, 033126 (2019).
[41] Yahya Alavirad and Jay Sau, "Ferromagnetism and its stability from the one-magnon spectrum in twisted bilayer graphene," Phys. Rev. B **102**, 235123 (2020).
[42] Jianpeng Liu and Xi Dai, "Theories for the correlated insulating states and quantum anomalous hall effect phenomena in twisted bilayer graphene," Phys. Rev. B **103**, 035427 (2021).
[43] Youngjoon Choi, Jeannette Kemmer, Yang Peng, Alex Thomson, Harpreet Arora, Robert Polski, Yiran Zhang, Hechen Ren, Jason Alicea, Gil Refael, *et al.*, "Electronic correlations in twisted bilayer graphene near the magic angle," Nature Physics **15**, 1174–1180 (2019).
[44] Simone Lisi, Xiaobo Lu, Tjerk Benschop, Tobias A de Jong, Petr Stepanov, Jose R Duran, Florian Margot, Irène Cucchi, Edoardo Cappelli, Andrew Hunter, *et al.*, "Observation of flat bands in twisted bilayer graphene," Nature Physics **17**, 189–193 (2021).
[45] Leon Balents, Cory R Dean, Dmitri K Efetov, and Andrea F Young, "Superconductivity and strong correlations in moiré flat bands," Nature Physics **16**, 725–733 (2020).
[46] T. M. R. Wolf, J. L. Lado, G. Blatter, and O. Zilberberg, "Electrically tunable flat bands and magnetism in twisted bilayer graphene," Phys. Rev. Lett. **123**, 096802 (2019).
[47] Martin Gmitra and Jaroslav Fabian, "Proximity Effects in Bilayer Graphene on Monolayer WSe_2: Field-Effect Spin Valley Locking, Spin-Orbit Valve, and Spin Transistor," Phys. Rev. Lett. **119**, 146401 (2017).
[48] Julia Amann, Tobias Völkl, Denis Kochan, Kenji Watanabe, Takashi Taniguchi, Jaroslav Fabian, Dieter Weiss, and Jonathan Eroms, "Gate-tunable spin-orbit-coupling in bilayer graphene-wse_2-heterostructures," arXiv:2012.05718 (2021).
[49] Klaus Zollner, Martin Gmitra, and Jaroslav Fabian, "Swapping exchange and spin-orbit coupling in 2d van der waals heterostructures," Phys. Rev. Lett. **125**, 196402 (2020).
[50] Jiang-Xiazi Lin, Ya-Hui Zhang, Erin Morissette, Zhi Wang, Song Liu, Daniel Rhodes, K. Watanabe, T. Taniguchi, James Hone, and J. I. A. Li, "Proximity-induced spin-orbit coupling and ferromagnetism in magic-angle twisted bilayer graphene," arXiv:2102.06566 (2021).
[51] Dongying Wang, Shi Che, Guixin Cao, Rui Lyu, Kenji Watanabe, Takashi Taniguchi, Chun Ning Lau, and Marc Bockrath, "Quantum Hall Effect Measurement of Spin–Orbit Coupling Strengths in Ultraclean Bilayer Graphene/WSe_2 Heterostructures," Nano Lett. **19**, 7028 (2019).
[52] J. O. Island, X. Cui, C. Lewandowski, J. Y. Khoo, E. M. Spanton, H. Zhou, D. Rhodes, J. C. Hone, T. Taniguchi, K. Watanabe, L. S. Levitov, M. P. Zaletel, and A. F. Young, "Spin-orbit-driven band inversion in bilayer graphene by the van der Waals proximity effect," Nature **571**, 85 (2019).
[53] C. Cardoso, D. Soriano, N. A. García-Martínez, and J. Fernández-Rossier, "Van der Waals Spin Valves," Phys. Rev. Lett. **121**, 067701 (2018).
[54] Priya Tiwari, Saurabh Kumar Srivastav, and Aveek Bid, "Electric-field-tunable valley zeeman effect in bilayer graphene heterostructures: Realization of the spin-orbit valve effect," Phys. Rev. Lett. **126**, 096801 (2021).
[55] Abdulrhman M. Alsharari, Mahmoud M. Asmar, and Sergio E. Ulloa, "Proximity-induced topological phases in bilayer graphene," Phys. Rev. B **97**, 241104 (2018).
[56] Amol Nimbalkar and Hyunmin Kim, "Opportunities and challenges in twisted bilayer graphene: a review," Nano-Micro Letters **12**, 126 (2020).
[57] S. Omar and B. J. van Wees, "Spin transport in high-mobility graphene on WS_2 substrate with electric-field tunable proximity spin-orbit interaction," Phys. Rev. B **97**, 045414 (2018).
[58] S. Omar, B. N. Madhushankar, and B. J. van Wees, "Large spin-relaxation anisotropy in bilayer-graphene/WS_2 heterostructures," Phys. Rev. B **100**, 155415 (2019).
[59] Bogdan Karpiak, Aron W. Cummings, Klaus Zollner, Marc Vila, Dmitrii Khokhriakov, Anamul Md Hoque, André Dankert, Peter Svedlindh, Jaroslav Fabian, Stephan Roche, and Saroj P. Dash, "Magnetic proximity in a van der Waals heterostructure of magnetic insulator and graphene," 2D Mater. **7**, 015026 (2019).
[60] Dmitrii Khokhriakov, Aron W. Cummings, Kenan Song, Marc Vila, Bogdan Karpiak, André Dankert, Stephan Roche, and Saroj P. Dash, "Tailoring emergent spin phenomena in Dirac material heterostructures," Sci. Adv. **4**, eaat9349 (2018).
[61] Anamul Md. Hoque, Dmitrii Khokhriakov, Bogdan Karpiak, and Saroj P. Dash, "All-electrical creation and control of giant spin-galvanic effect in 1t-$mote_2$/graphene heterostructures at room temperature," arXiv:1908.09367 (2019).
[62] Tobias Frank, Martin Gmitra, and Jaroslav Fabian, "Theory of electronic and spin-orbit proximity effects in graphene on Cu(111)," Phys. Rev. B **93**, 155142 (2016).
[63] Võ Tien Phong, Niels R Walet, and Francisco Guinea, "Effective interactions in a graphene layer induced by the proximity to a ferromagnet," 2D Mater. **5**, 014004 (2017).
[64] Zhenhua Qiao, Wei Ren, Hua Chen, L. Bellaiche, Zhenyu Zhang, A. H. MacDonald, and Qian Niu, "Quantum Anomalous Hall Effect in Graphene Proximity Coupled to an Antiferromagnetic Insulator," Phys. Rev. Lett. **112**, 116404 (2014).
[65] Johannes Christian Leutenantsmeyer, Alexey A Kaverzin, Magdalena Wojtaszek, and Bart J van Wees, "Proximity induced room temperature ferromagnetism in graphene probed with spin currents," 2D Mater. **4**, 014001 (2016).
[66] Simon Zihlmann, Aron W. Cummings, Jose H. Garcia, Máté Kedves, Kenji Watanabe, Takashi Taniguchi, Christian Schönenberger, and Péter Makk, "Large spin relaxation anisotropy and valley-Zeeman spin-orbit coupling in WSe_2/graphene/h-BN heterostructures," Phys. Rev. B **97**, 075434 (2018).
[67] Talieh S. Ghiasi, Josep Ingla-Aynés, Alexey A. Kaverzin, and Bart J. Van Wees, "Large Proximity-Induced Spin Lifetime Anisotropy in Transition-Metal Dichalcogenide/Graphene Heterostructures," Nano Lett. **17**, 7528 (2017).

[68] S. Jafarpisheh, A. W. Cummings, K. Watanabe, T. Taniguchi, B. Beschoten, and C. Stampfer, "Proximity-induced spin-orbit coupling in graphene/$Bi_{1.5}Sb_{0.5}Te_{1.7}Se_{1.3}$ heterostructures," Phys. Rev. B **98**, 241402 (2018).

[69] Zhiyong Wang, Chi Tang, Raymond Sachs, Yafis Barlas, and Jing Shi, "Proximity-Induced Ferromagnetism in Graphene Revealed by the Anomalous Hall Effect," Phys. Rev. Lett. **114**, 016603 (2015).

[70] H. X. Yang, A. Hallal, D. Terrade, X. Waintal, S. Roche, and M. Chshiev, "Proximity Effects Induced in Graphene by Magnetic Insulators: First-Principles Calculations on Spin Filtering and Exchange-Splitting Gaps," Phys. Rev. Lett. **110**, 046603 (2013).

[71] Ali Hallal, Fatima Ibrahim, Hongxin Yang, Stephan Roche, and Mairbek Chshiev, "Tailoring magnetic insulator proximity effects in graphene: first-principles calculations," 2D Mater. **4**, 025074 (2017).

[72] T. Wakamura, F. Reale, P. Palczynski, M. Q. Zhao, A. T. C. Johnson, S. Guéron, C. Mattevi, A. Ouerghi, and H. Bouchiat, "Spin-orbit interaction induced in graphene by transition metal dichalcogenides," Phys. Rev. B **99**, 245402 (2019).

[73] Shaowen Chen, Minhao He, Ya-Hui Zhang, Valerie Hsieh, Zaiyao Fei, K Watanabe, T Taniguchi, David H Cobden, Xiaodong Xu, Cory R Dean, *et al.*, "Electrically tunable correlated and topological states in twisted monolayer–bilayer graphene," Nature Physics **17**, 374–380 (2021).

[74] S. R. Bahn and K. W. Jacobsen, "An object-oriented scripting interface to a legacy electronic structure code," Comput. Sci. Eng. **4**, 56 (2002).

[75] Koichi Momma and Fujio Izumi, "VESTA3 for three-dimensional visualization of crystal, volumetric and morphology data," J. Appl. Cryst. **44**, 1272 (2011).

[76] W. J. Schutte, J. L. De Boer, and F. Jellinek, "Crystal structures of tungsten disulfide and diselenide," J. Solid State Chem. **70**, 207 (1987).

[77] V Carteaux, D Brunet, G Ouvrard, and G Andre, "Crystallographic, magnetic and electronic structures of a new layered ferromagnetic compound $Cr_2Ge_2Te_6$," J. Phys.: Condens. Mat. **7**, 69 (1995).

[78] P. Hohenberg and W. Kohn, "Inhomogeneous Electron Gas," Phys. Rev. **136**, B864 (1964).

[79] Paolo Giannozzi, Stefano Baroni, Nicola Bonini, Matteo Calandra, Roberto Car, Carlo Cavazzoni, Davide Ceresoli, Guido L Chiarotti, Matteo Cococcioni, Ismaila Dabo, Andrea Dal Corso, Stefano de Gironcoli, Stefano Fabris, Guido Fratesi, Ralph Gebauer, Uwe Gerstmann, Christos Gougoussis, Anton Kokalj, Michele Lazzeri, Layla Martin-Samos, Nicola Marzari, Francesco Mauri, Riccardo Mazzarello, Stefano Paolini, Alfredo Pasquarello, Lorenzo Paulatto, Carlo Sbraccia, Sandro Scandolo, Gabriele Sclauzero, Ari P Seitsonen, Alexander Smogunov, Paolo Umari, and Renata M Wentzcovitch, "QUANTUM ESPRESSO: a modular and open-source software project for quantum simulations of materials," J. Phys.: Cond. Mat. **21**, 395502 (2009).

[80] G. Kresse and D. Joubert, "From ultrasoft pseudopotentials to the projector augmented-wave method," Phys. Rev. B **59**, 1758 (1999).

[81] John P. Perdew, Kieron Burke, and Matthias Ernzerhof, "Generalized Gradient Approximation Made Simple," Phys. Rev. Lett. **77**, 3865 (1996).

[82] Cheng Gong, Lin Li, Zhenglu Li, Huiwen Ji, Alex Stern, Yang Xia, Ting Cao, Wei Bao, Chenzhe Wang, Yuan Wang, Z. Q. Qiu, R. J. Cava, Steven G. Louie, Jing Xia, and Xiang Zhang, "Discovery of intrinsic ferromagnetism in two-dimensional van der Waals crystals," Nature **546**, 265 (2017).

[83] Stefan Grimme, "Semiempirical GGA-type density functional constructed with a long-range dispersion correction," J. Comput. Chem. **27**, 1787 (2006).

[84] Vincenzo Barone, Maurizio Casarin, Daniel Forrer, Michele Pavone, Mauro Sambi, and Andrea Vittadini, "Role and effective treatment of dispersive forces in materials: Polyethylene and graphite crystals as test cases," J. Comput. Chem. **30**, 934 (2009).

[85] Lennart Bengtsson, "Dipole correction for surface supercell calculations," Phys. Rev. B **59**, 12301 (1999).

[86] S. Konschuh, M. Gmitra, D. Kochan, and J. Fabian, "Theory of spin-orbit coupling in bilayer graphene," Phys. Rev. B **85**, 115423 (2012).

[87] Denis Kochan, Susanne Irmer, and Jaroslav Fabian, "Model spin-orbit coupling Hamiltonians for graphene systems," Phys. Rev. B **95**, 165415 (2017).

[88] See Supplemental Material, where we show a more extended comparison between the DFT results and the model band structure, splittings, and spin expectation values. In addition, we show the calculated charge density from the low energy bands in real space.

[89] M. Gmitra, S. Konschuh, C. Ertler, C. Ambrosch-Draxl, and J. Fabian, "Band-structure topologies of graphene: Spin-orbit coupling effects from first principles," Phys. Rev. B **80**, 235431 (2009).

[90] Sergej Konschuh, Martin Gmitra, and Jaroslav Fabian, "Tight-binding theory of the spin-orbit coupling in graphene," Phys. Rev. B **82**, 245412 (2010).

[91] Xu-Dong Chen, Wei Xin, Wen-Shuai Jiang, Zhi-Bo Liu, Yongsheng Chen, and Jian-Guo Tian, "High-precision twist-controlled bilayer and trilayer graphene," Advanced Materials **28**, 2563–2570 (2016).

[92] Edward McCann and Mikito Koshino, "The electronic properties of bilayer graphene," Rep. Prog. Phys. **76**, 056503 (2013).

[93] Aron W. Cummings, Jose H. Garcia, Jaroslav Fabian, and Stephan Roche, "Giant Spin Lifetime Anisotropy in Graphene Induced by Proximity Effects," Phys. Rev. Lett. **119**, 206601 (2017).

Supplemental Material: Bilayer graphene encapsulated within monolayers of WS_2 or $Cr_2Ge_2Te_6$: Tunable proximity spin-orbit or exchange coupling

Klaus Zollner[1,*] and Jaroslav Fabian[1]

[1] *Institute for Theoretical Physics, University of Regensburg, 93040 Regensburg, Germany*

In the Supplemental Material we again show the band structure of the WS_2 encapsulated BLG for the 0° twist angle case, including the model Hamiltonian fit. Here, we explicitly show that also the high energy bands, spin splittings, and spin expectation values are in good agreement with the model Hamiltonian fit. In addition, we show the DFT-calculated charge density in real space, corresponding to the low energy bands near the Fermi level.

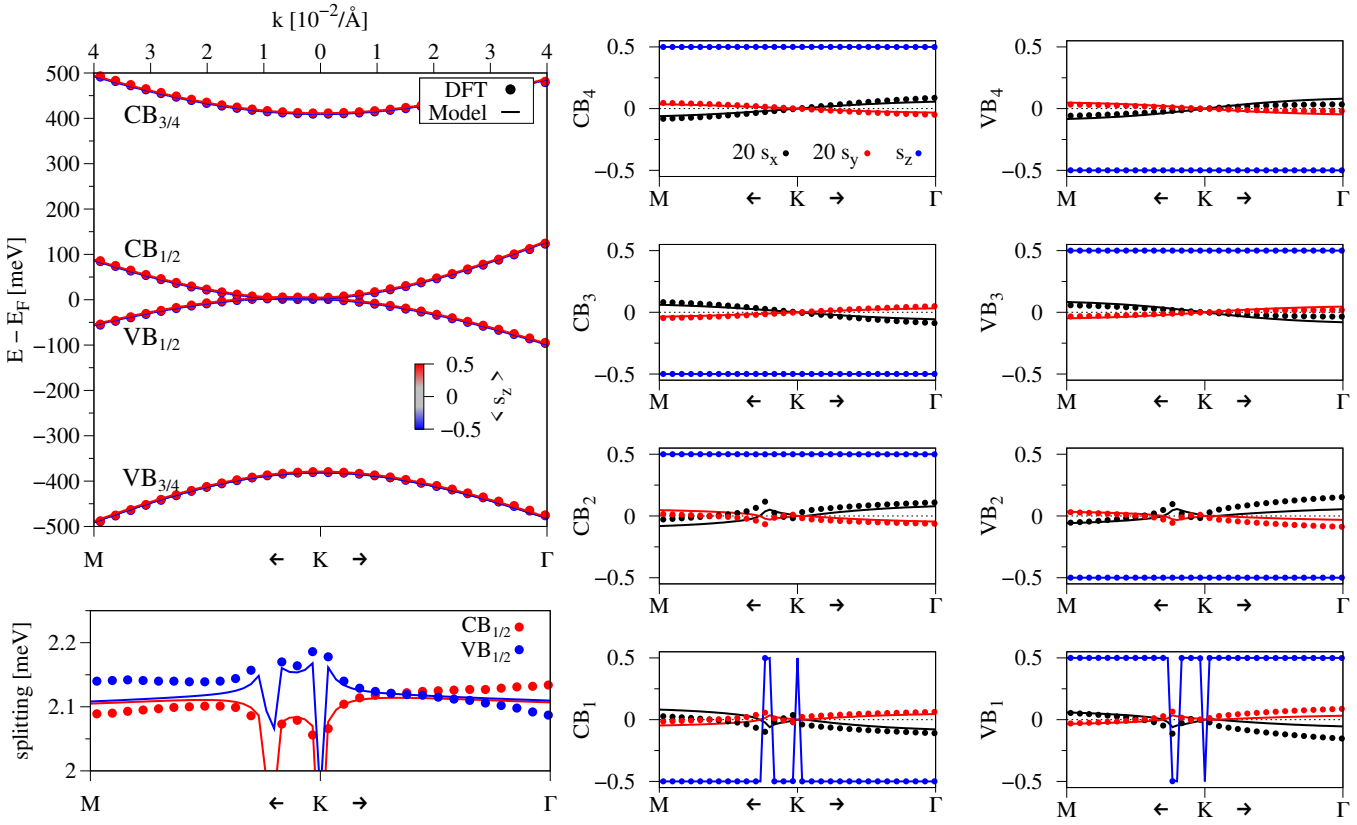


FIG. S1. DFT-calculated band structure (symbols) of WS_2 encapsulated BLG for the 0° twist angle case, including the fit to the model Hamiltonian (solid lines). Here, we show all 8 bands belonging to BLG, which are in good agreement with the model. The color of the bands corresponds to the s_z spin expectation value. Also the band splittings and their spin expectation values (s_x, s_y, and s_z) agree well with the model. The in-plane spin expectation values are multiplied by a factor of 20 for better visualization.

* klaus.zollner@physik.uni-regensburg.de

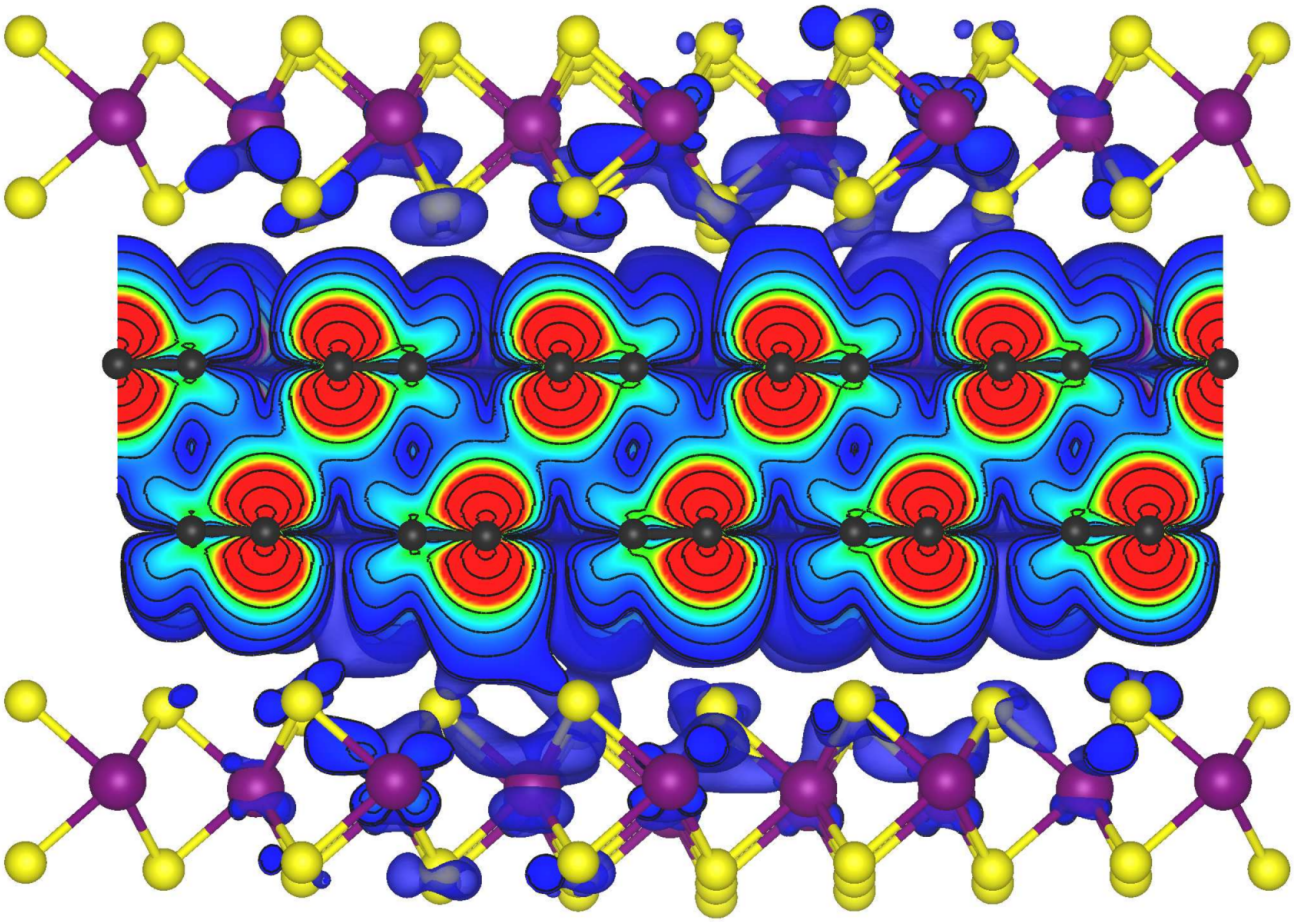


FIG. S2. DFT-calculated integrated local density of states of the WS_2 encapsulated BLG for the 0° twist angle case. We take into account only states in an energy window of ±25 meV around the Fermi level from the band structure in Fig. S1. The colors correspond to isovalues between 2×10^{-4} (red) and 3×10^{-6} (blue) e/Å^3, while the isolines range from 1×10^{-2} to 1×10^{-6} e/Å^3.